Tracing the Iceland plume and North East Atlantic breakup in the lithosphere

Maria Laura Gomez Dacal (gomezdacal@fcaglp.unlp.edu.ar)
Universidad Nacional de La Plata https://orcid.org/0000-0003-0504-2018
Magdalena Scheck-Wenderoth
GeoForschungsZentrum Potsdam
Jan Inge Faleide
University of Oslo
Mohamed Mansour Abdelmalak
Department of Geosciences, University of Oslo
Judith Bott
HelmholtzZentrum GFZ - German Research Centre for Geosciences https://orcid.org/0000-0002-2018-4754
Denis Anikiev
Helmholtz Centre Potsdam – GFZ German Research Centre for Geosciences

Article

Keywords:

Posted Date: May 29th, 2023

DOI: https://doi.org/10.21203/rs.3.rs-2845593/v1

Additional Declarations: There is **NO** Competing Interest.

Version of Record: A version of this preprint was published at Communications Earth & Environment on December 6th, 2023. See the published version at https://doi.org/10.1038/s43247-023-01120-w.

Tracing the Iceland plume and North East Atlantic breakup in the lithosphere

María Laura Gomez Dacal[1], Magdalena Scheck-Wenderoth[2,3], Jan Inge Faleide[4], Mohamed Mansour Abdelmalak[4], Judith Bott[2], Denis Anikiev[2]

1 National University of La Plata. Faculty of Astronomical and Geophysical Sciences. Paseo del Bosque. B1900FWA, La Plata, Argentina.
2 Helmholtz Centre Potsdam – GFZ German Research Centre for Geosciences. Telegrafenberg. 14473, Potsdam, Germany.
3 RWTH Aachen, Faculty of Georesources and Materials Engineering. Lochnerstr. 4-20, 52056 Aachen, Germany
4 Department of Geosciences, University of Oslo. Sem Sælands vei 2A, Blindern. N-0371, Oslo, Norway.

Abstract

Plumes are domains where hotter material rises through Earth´s mantle, heating also the moving lithospheric plates and causing thinning or even continental breakup. In particular, the Iceland plume in the NE Atlantic (NEA) could have been instrumental in facilitating the breakup between Europe and Laurentia in the earliest Eocene, 55 Ma. This hypothesis relies on different observations that have not yet been integrated into a quantitative description of the present-day geophysical configuration. Here we show, for the first time, an open access three-dimensional model of the entire NEA crust and upper mantle including the conjugate continental margins of Greenland and Norway, as well as the sheared margins of the northernmost NEA. The model is consistent with available seismic, seismological and gravity data. We propose that high-density/high-velocity anomalies in the crust represent the preserved modifications of the lithosphere in consequence of the plate's journey over the hot mantle plume. Besides, low-density/low-velocity anomalies in the uppermost mantle would represent the present-day effect of the mantle plume and its interaction with the mid-ocean ridges. Overall, the model indicates that the presence of the plume together with the pre-existing crustal configuration controlled the timing, mechanisms and localization of the NEA breakup.

Main

Agreement has been reached recently that mechanisms behind continental breakup and passive margin formation encompass a continuum between mantle-driven/magma-rich and plate-driven/magma-poor deformation[1-4]. Three-dimensional thermo-dynamic modelling studies considering magmatism[1,2] demonstrated that mantle plumes can support continental breakup considerably if the plume meets a plate under orthogonal extension and that this can lead to the formation of magma-rich continental margins. On the other hand, dynamic three-dimensional modelling studies[3,4] have also demonstrated that plate-driven lithospheric breakup in absence of magma is more difficult in orthogonal extension than with some degree of obliquity. In such magma-poor settings, deformation is accommodated in simple shear leading even to mantle exhumation at the oceanic side of large-offset listric faults. In both end-member settings, variations in thickness, architecture and rheology of the lithosphere is of key importance for the breakup dynamics.

In the NE Atlantic (NEA), successful breakup between Greenland and Eurasia at about 55 Ma was preceded by a long history of near-orthogonal (to the main structures) extensional deformation. The extensional setting, present from late Paleozoic times onward, created deep sedimentary basins but did not succeed in breaking the plates apart. Accordingly, the domains composing the present-day passive continental margins of the NEA host up to 12 km thick Cretaceous to Paleocene sedimentary units and additional several km of pre-Cretaceous deposits[5-7]. However, the orientation of the breakup axis is oblique to the pre-existing Paleozoic/Mesozoic rift structures of the NEA and resulted in voluminous extrusive and intrusive igneous activities[8].

In the course of this extensional history, both breakup end-members seem to have played a role and a magma-rich setting is characterizing the central part of the system at the latitude of Iceland that transitions to a less magmatic setting to the north and south. The weakening influence of a hot mantle plume is one explanation suggested for why breakup eventually succeeded. This hypothesis is also supported by reconstructions of paleo plate configurations[9-11] and a generally thinner lithosphere beneath central Greenland interpreted as resulting from westward movement of Greenland over a thermal mantle plume[12-14].

The questions that remain are which role the Iceland plume has played in facilitating continental breakup between Eurasia and Greenland/North America, and which traces of these processes can be detected in the present-day configuration of the crust and mantle in the region. Major focuses of disputes are the nature of the crust composing present-day Greenland-Iceland-Faroe Ridge (GIFR; e.g. [15]), the nature and origin of high-velocity/high-density bodies in the lower crust of the conjugate passive continental margins[16,17] and the nature and origin of the locally thickened magmatic oceanic crust along an E-W trending domain on both sides of Iceland (GIFR), also characterized by high seismic velocities[18,19]. In addition, there are several lines of disagreement related to the causes behind breakup 55 Million years ago along a line cutting diagonally domains of previous crustal thinning (e.g.[6]).

Though the amount of geoscientific observations has increased steadily over the past decades, integration into one consistent model representation is still lacking. With this work, we for the first time, present a three-dimensional model of the NEA (location in Fig. 1) that resolves the major structural characteristics of the crust and uppermost mantle based on the integration of multidisciplinary geological and geophysical observations - seismic profiles, depth and thickness maps, existing models, seismic mantle tomography - and forward and inverse gravity modelling (for details see Methods, Supplementary Information -SI- and Extended Data: Figures 1, 2 and Table 1). We, moreover, discuss how the model contributes to the ongoing debates in this geodynamically complex area.

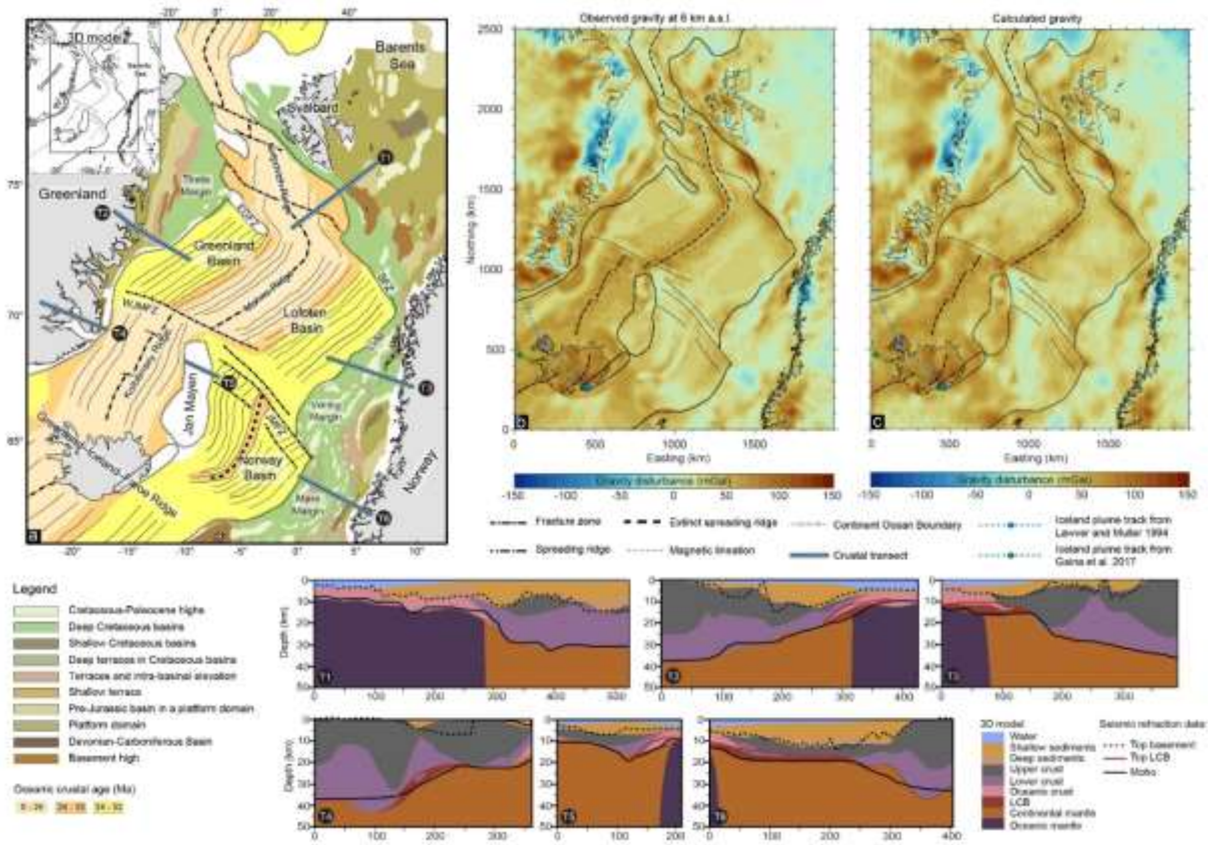

Figure 1: Model area and examples of constraining data and model fitting. a) Simplified structural map of the modelled area. The location of the 3D model is shown on the upper left corner. Black and blue lines mark the locations of the crustal transects (bottom of the figure), denoted as T1-6. Transects illustrate the variations in structural configuration and the consistence with input deep seismic refraction data[8]; b) Free air gravity disturbance over the NE Atlantic region at 6 km above sea level from EIGEN-6C4[20,21]; c) Calculated gravity response of the model at 6 km above sea level. The gravity response of the 3D model as a whole generally fits the observed gravity very well. The larger misfits are of high frequency, indicating some features of the area that the model is not able to resolve according to its structural resolution. Further information on all considered input data as well as explanations of remaining gravity residuals and their relation to model limitations are presented in the Supplementary Information (SI).

Variation of lithospheric configuration

The modelled three-dimensional lithospheric configuration (Fig. 2) illustrates four main characteristics: (1) lithosphere thickness varies between less than 50 km in the oceanic and more than 250 km in the continental regions (Fig. 2j); (2) the crust is thickest (>35 km; Fig. 2e) below the continental domains and along the GIFR as imaged by the variations in Moho depth (Fig. 2c), (3) the crust encompasses thick successions (up to 21 km) of sediments (Fig. 2d) underlain by a two-layered crystalline crust (Figs. 2f and g); (4) presence of high-density/high-velocity lower crustal bodies (Figs. 2i) along the continent-ocean transition (COT), particularly in the central part of the NEA, and along the GIFR. More details about the final model can be observed in the Extended Data (Extended data Figures 3 and 4 and Extended data Table 2).

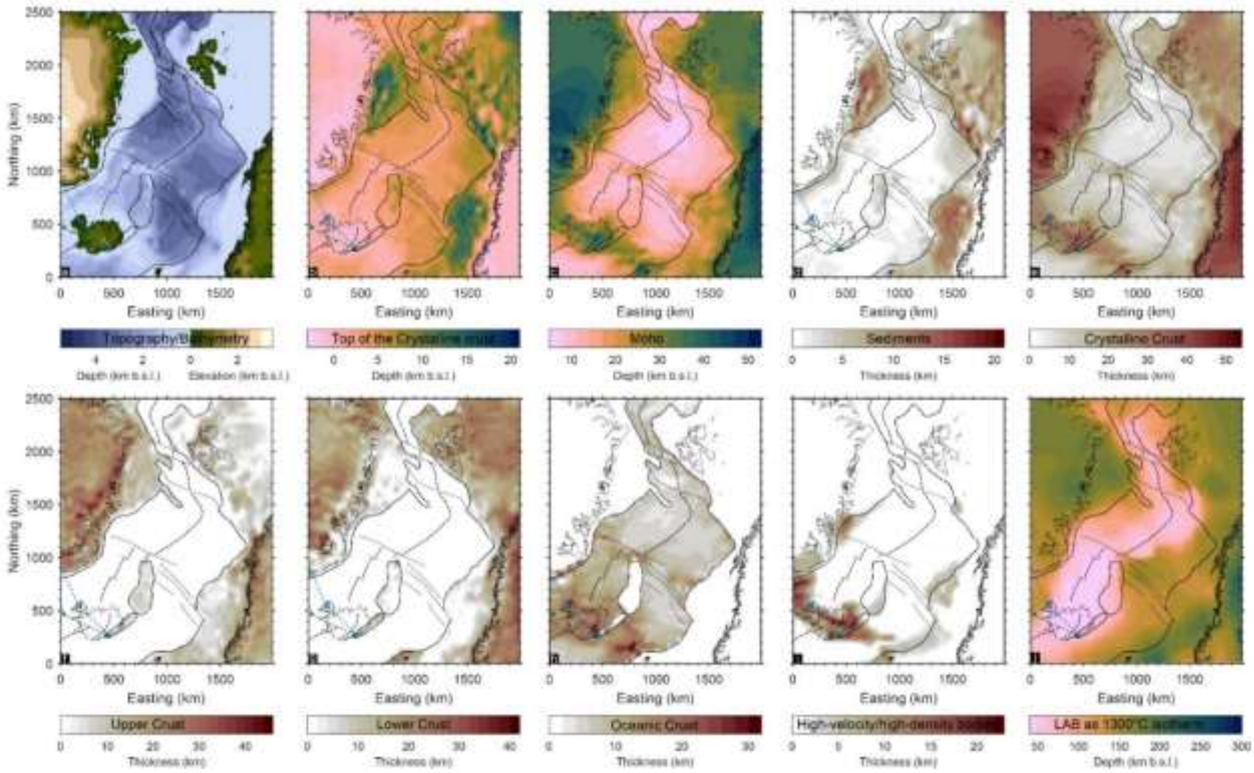

Figure 2: Major structural characteristics of the 3D model. Upper panel: surfaces and thicknesses compiled from different data sources; lower panel: structures derived by forward and inverse gravity modelling (f-i) or the conversion of tomographic data (j). More illustrations, details and references on data sources and integration methods provided in Methods and the SI. a) Topography of the elevated areas, including the ice surface in glacial areas (Greenland) and bathymetry in the ocean (ETOPO 1[22]); b) Depth to the top of the crystalline basement c) Depth to Moho d) Thickness of the sedimentary layer; e) Thickness of the crystalline crust; f) Thickness of the upper felsic crystalline continental crust characterized by average velocities of ~5.8 km/s to ~6.5 km/s and an average density of 2700 kg/m3; g) Thickness of the lower mafic crystalline continental crust characterized by average velocities of ~6.5 to 7 km/s and an average density of 3000 kg/m3; h) Thickness of the oceanic crust with an average density of 2900 kg/m3; i) Thickness of the lower crustal high-velocity/high-density bodies, characterized by average velocities > 7 km/s and an average density of 3000 kg/m3 at the passive continental margins near the COT (COT-LCB; derived from [17]) and by an average density of 3100 kg/m3 along the GIRF (GIFR layer 3) as derived by forward gravity modelling; j) Depth to the thermal Lithosphere-Asthenosphere Boundary (LAB) extracted as the 1300 °C isotherm from the temperature distribution obtained by velocity conversion[23] of the shear wave tomography[24]. Green and blue stippled lines are the previously proposed tracks of the Iceland plume [25, 26].

As imaged along the cross sections in Fig. 1, the continental crystalline crust consists of an upper unit, characterized by lower average velocities and densities, interpreted as an indication for a felsic composition and a lower unit, characterized by higher seismic velocities and densities, interpreted as mafic. Both the upper felsic crust and the lower mafic crust have a thickness ranging between ~10 km and 40 km (Fig. 2f and g). They are thickest below the onshore parts of the continental margins and thin considerable below the regions where crustal thinning is most severe towards the continent ocean boundary (COB) or along the Cretaceous basins. Oceanward, the COT is characterized by the occurrence of high-velocity/high-density lower crustal bodies (COT-LCBs) interpreted as a complex mixture of pre- to syn-breakup mafic and ultramafic rocks and old metamorphic rocks (e.g. [17,16]). Laterally, the COT-LCBs merge with the lowermost layer of the oceanic crust (layer 3) contributing to a thicker than normal oceanic crust, in particular in the area of GIFR (GIFR layer 3; Fig. 2i).

Over most of the oceanic domains, the average density distribution of the crystalline crust (Fig. 3a) is uniform, apart from the regions where high-velocity/high-density bodies are present. Particularly, the higher-than-normal density area of the GIFR correlates spatially with a thicker-than-normal oceanic crust (Figs. 2h and i). In the continental domains, the average crustal density varies between 2700 kg/m3 and 3100 kg/m3, depending on the modelled local proportion of upper and lower crust (see Methods and SI) and on the presence of high-density COT-LCBs (Figs. 2f, g and i). Accordingly, higher average densities of the crystalline crust are found below the continental margins where the COT-LCBs are present and below the Barents Sea, a region also characterized by an increased thickness of the crystalline crust (Figs. 3a and 2e). In contrast, the average crustal density is far lower below the largest parts of Greenland than below the Barents Sea and below onshore Norway. The average density of the continental domain is lower west of the Atlantic than to the east suggesting that the Greenland-American lithosphere had different properties compared to the Eurasian lithosphere and that the breakup may have occurred where a corresponding contrast in mechanical properties was present. This contrast is more pronounced in the northern part of the model, in the sheared margin domain (between northern offshore Greenland and the Barents Sea), coinciding with the area where the break-up related magmatism is less abundant[27]. More details on the crustal density distribution are found in the Extended data Figure 5.

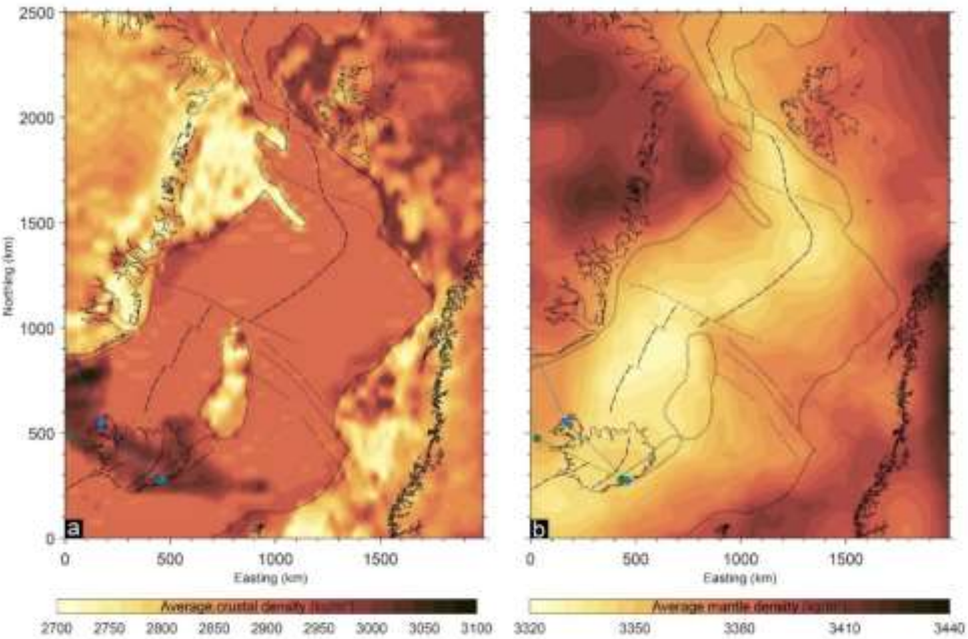

Figure 3. First-order density configuration of the model: a) average density of the crystalline crust; b) average density of the upper mantle between the Moho and 300 km depth. Green and blue stippled lines are the proposed tracks of the Iceland plume obtained from two different sources, [25] and [26], respectively. More details and figures of the mantle density and temperature distribution can be found in the SI.

The first-order characteristics of the mantle configuration have been obtained by converting the mantle shear wave velocities[24] to temperatures and densities ([28] and references therein, see Methods, SI and Extended Data Figure 6). The derived densities were used to calculate the average mantle density distribution (Fig. 3b) that illustrates a long-wavelength variation between the oceanic domain, with generally lower mantle average densities, and the continental domain with higher average densities of the mantle. Lower-than-average mantle densities in response to higher-than-average mantle temperatures characterize a wide region below the mid oceanic ridge (MOR), including Iceland (Fig. 3b). These low-density areas in the mantle coincide with an elevated Moho below the MOR (Fig. 2c). Only below Iceland and its surroundings (GIFR), where the oceanic crust is thicker than normal, the mantle is, nevertheless, light and warm. The lowest average density is located below the Kolbeinsey Ridge, north of Iceland. In contrast, the coldest mantle temperatures in the oceanic domain correspond to the oldest oceanic areas offshore NE Greenland and offshore mid-Norway and are also characterized by higher-than-average densities (Fig. 3b). Within the continental domain, the coldest mantle temperatures of the model area, correlating with the highest average mantle densities, are calculated for the larger parts below NE Greenland, the eastern Barents Sea and onshore Norway.

In the central portion of the NEA (Fig. 1a), seismological evidence[12,24,29] reveals a low shear wave velocity anomaly indicative for higher-than-average temperatures in the uppermost mantle. This observation, together with the elevated topography of Iceland compared to other parts of the Mid Atlantic Ridge (Fig. 2a), were the main arguments for assuming a mantle plume beneath Iceland[29-31]. Analysing the mantle-velocity-derived temperatures and densities in detail reveals that the mantle is hottest/lightest beneath Iceland to a depth of 50 km. Below this level, between 50 and 100 km depth, the domain of the high-temperature/low-density anomaly extends north to also include the region below the Kolbeinsey Ridge, west of the Jan Mayen microcontinent (Fig.4). Moving downwards, below 100 km depth, the anomaly locates only beneath the Kolbeinsey Ridge, whereas the temperature increase is less pronounced below Iceland. Thus, a continuous thermal anomaly (low-density body) from the shallow interval to larger depths can be traced only north of Iceland and connects the shallow Iceland anomaly to the one beneath the mid ocean Kolbeinsey Ridge. Thus, Iceland itself is located above a southward protrusion of the thermal anomaly rising continuously vertically along the Kolbeinsey Ridge from more than 200 km depth (Fig. 4a).

Only the mantle configuration in the central part of the NEA, with its wide region of low density (Fig. 3b, 4a), is accompanied by magma-rich passive rifted margins on either side whereas less magmatic margin segments prevail towards the south and north. Particularly, the 3D model illustrates the correlation between the colder/denser mantle and the less magmatic setting at the northern NEA margin also coinciding with a change in opening regime from an orthogonal passive margin in the central part to a sheared margin in the north. The only low-density/low-velocity anomaly in the northern NEA is a smaller-scale feature observed from 140 km to 220 km depth north of the Knipovich Ridge (Fig. 4; see SI and Extended Data Figure 7).

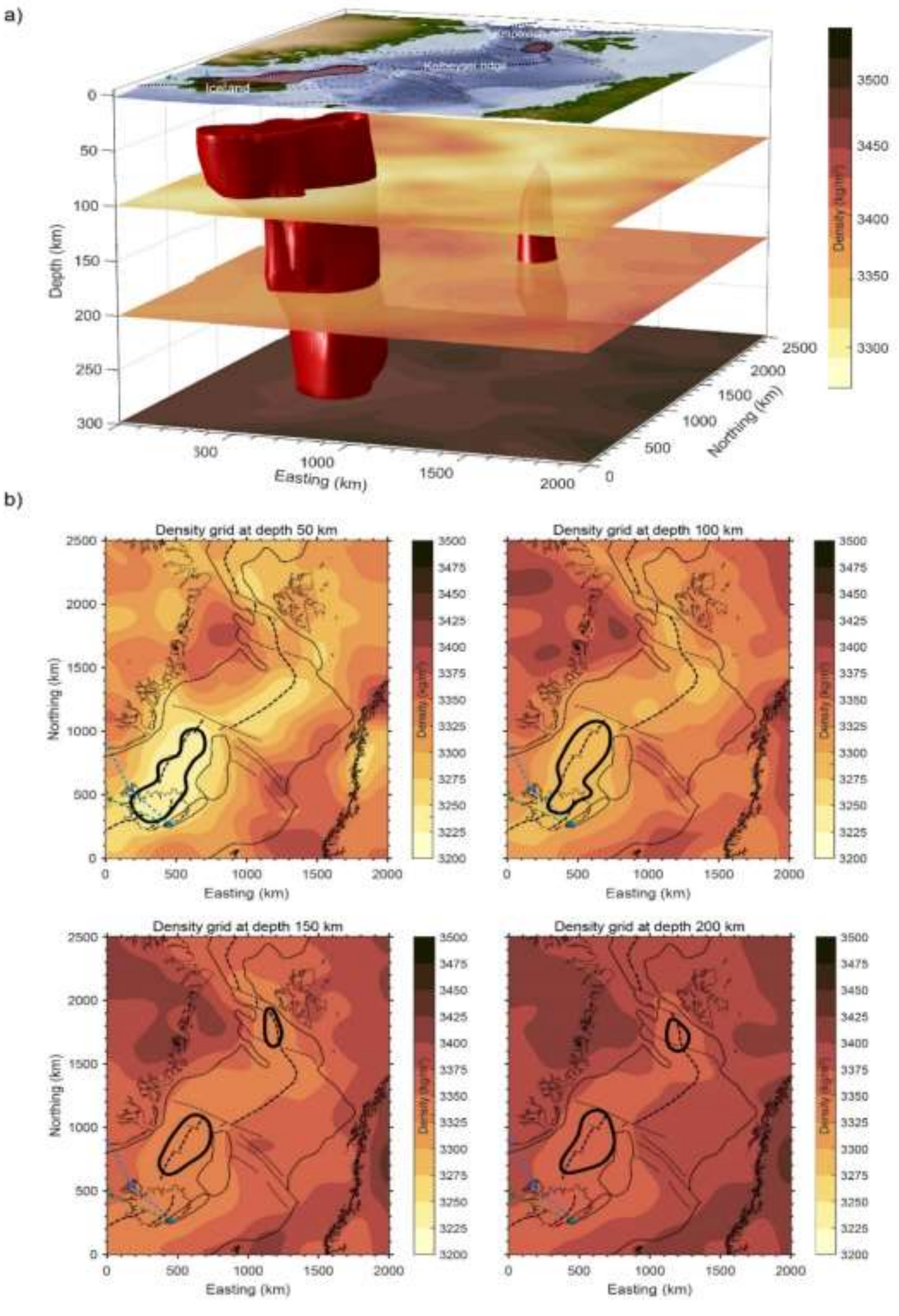

Figure 4. Detailed mantle density structure. a) 3D image of a low-density body in the mantle statistically delimited by the 1st percentile of the lowest densities. b) Depth slices of density distribution at 50 km depth intervals. The black curves show the location of the 1st percentile of lowest densities at each depth.

Dynamic implications

The three-dimensional density configuration of the crust and upper mantle in the NEA reveals the traces left by the breakup of a continental plate in response to extension and plume-lithosphere interactions. On both sides of the NEA, the normal-faulted passive continental margins prove that extensional stresses have influenced the breakup process. That several extensional phases in the Mesozoic did not succeed in continental breakup has been explained by different mechanisms[7,32-34]. Among others, discussed reasons for unsuccessful breakup before the Eocene include: (i) insufficiently large extension to break a thick and strong lithosphere; (ii) strain hardening of the rifted domains in response to the rifting velocity being slower than conductive cooling of the rifting-related thermal anomaly; or (iii) cessation of extensional forcing before breakup. That rifting was successful in the earliest Eocene, in spite of rather minor extension, could be explained as being due to additional support by a thermal anomaly in the mantle[35]. Such dynamic support by a buoyant hot mantle would also be consistent with the presence of an erosional breakup unconformity on both passive margins. The unconformity documents that these domains have been uplifted shortly before or syn-breakup, right after a phase of deep marine conditions in the late Cretaceous-early Paleocene[36]. Finally, the presence of large volumes of magmatic products near the COT of the central NEA (Fig. 2i) prove that the breaking lithosphere was hot. Such magmatic products are documented in the deeper crust as COT-LCBs (Fig. 2i), as sill intrusions in the sedimentary basins and as surface volcanic extrusives, including basaltic flows penetrated by several boreholes offshore Norway[37]. The amount of magmatism per se is difficult to explain without a plume[38]. Besides, the associated elevated mantle temperatures/low densities (Figs. 3b and 4), as well as the shallower than normal NEA bathymetry (Fig. 2a) compared to a plate cooling model[39], both require the activity of a mantle plume. That the magmatic crust is both thicker (Fig. 2e; see also [47]) and denser than normal (Fig. 3a) in the oceanic area along the GIFR and that this region coincides spatially with the track of the Iceland plume reconstructed by independent methods[25,26] is the cherry on the cake of our findings. It is this latter finding that strongly supports the arrival of the mantle plume and its subsequent track in the moving plates above.

The contrasting hypothesis that the Icelandic crust is continental[15] is not supported by our model. To achieve consistence with observed gravity (Fig. 1b), rather high average crustal densities in the region of Iceland are required that are far higher than typical continental crustal densities (Fig. 3a). As seismic tomography demonstrates that the GIFR area is characterized by low mantle densities (Fig. 3b), the upper mantle cannot balance the mass deficit either. Therefore, the contribution to the required gravity response has to come from the crust. We cannot exclude, however, that continental blocks may be baked into the mélange of magmatic products formed during the breakup process[10], in particular when associated with rift jumps[40,41].

Another interesting finding is a general difference in average density of the crust for the continental domain of Norway compared to the one of Greenland, at margins that are corresponding conjugates (Fig. 3a). To the north of the magma-rich central NEA margin, a change in regime is observed switching to a less magmatic sheared margin. The model indicates that the crust also contains less high-velocity/high-density bodies toward the North. In the less magmatic domain also the highest contrast of crustal average density between both corresponding conjugate margins (Fig. 3a) is detected. Considering the larger distance of the sheared margin to the plume, the latter was less influential in this region and accordingly less magmatic products are observed. This suggests that the localization of the rupture may have been guided by an ancient difference in rheology between the two plates for which the modelled large contrast in average crustal density could be an indication. These characteristics may have defined the opening regime of oblique extension as a preferred mechanism in a plate-driven breakup setting[3,4].

The mantle velocity-temperature-density configuration additionally correlates spatially with features observed at present-day in the area: regions of high temperature and low density correlate with the current plume position (as derived from [25] and [26]) and the MOR, especially to the north of Iceland (Kolbeinsey Ridge). Particularly, the lower than normal average densities of the model are arranged in a body that is located below the centre of Iceland at shallow depths, coinciding with the track of the plume of the last 20 Ma (Fig. 4). However, its continuation in depth is found beneath the Kolbeinsey Ridge (see also[29,42]), thus differing from the expected vertically continuous conduit-type shape of a plume. This could be an expression of the interaction of the plume with the MOR (see also[43]) changing abruptly along the Jan Mayen Fracture Zone[44,45]. Several tomography models, (e.g. [43,46]) coincide in the observation of low velocity anomalies that are related to two or more separate hotspots located along the MOR between the Reykjanes Ridge and the northern Kolbeinsey Ridge though the breadth of the inferred hot anomaly may vary between models. Common to most of the existing tomography models, however, is that distinct anomalies at shallowest mantle depths tend to merge into a single low-velocity anomaly at larger upper mantle depths.

In summary, the geophysical lithospheric configuration of the NEA, derived from various observations, demonstrates that the continental and oceanic crust preserved different aspects of the NEA history including several phases of extension, the thermal and magmatic imprints of the arriving mantle plume during and after the plate breakup and the subsequent cooling. The crust also preserved the changes in opening regime in response to the increasing distance to the plume, expressed as a transition between a magma-rich margin formation close to the plume and a less magmatic sheared margin setting at larger distance from the plume. In contrast, the upper mantle structure images the geodynamic processes active today, and their interactions:

vertically continuous domains of lower densities and higher temperatures below the present-day MOR and shallow mantle levels below Iceland point to a less important role of the plume today as compared to an increasingly stronger influence of the MOR anomaly.

Main references

1 Burov, E. & Gerya, T. Asymmetric three-dimensional topography over mantle plumes. *Nature* **513**, 85-89, doi:10.1038/nature13703 (2014).

2 Koptev, A., Ehlers, T. A., Nettesheim, M. & Whipp, D. M. Response of a rheologically stratified lithosphere to subduction of an indenter-shaped plate: Insights into localized exhumation at orogen syntaxes. *Tectonics* **38**, 1908-1930 (2019).

3 Brune, S., Popov, A. A. & Sobolev, S. V. Modeling suggests that oblique extension facilitates rifting and continental break-up. *Journal of Geophysical Research: Solid Earth* **117** (2012).

4 Le Pourhiet, L. *et al.* Continental break-up of the South China Sea stalled by far-field compression. *Nature Geoscience* **11**, 605-609 (2018).

5 Zastrozhnov, D. *et al.* Regional structure and polyphased Cretaceous-Paleocene rift and basin development of the mid-Norwegian volcanic passive margin. *Marine and Petroleum Geology* **115**, 104269 (2020).

6 Gernigon, L. *et al.* A digital compilation of structural and magmatic elements of the Mid-Norwegian continental margin (version 1.0). *Norwegian Journal of Geology/Norsk Geologisk Forening* **101** (2021).

7 Scheck-Wenderoth, M., Raum, T., Faleide, J., Mjelde, R. & Horsfield, B. The transition from the continent to the ocean: a deeper view on the Norwegian margin. *Journal of the Geological Society* **164**, 855-868 (2007).

8 Abdelmalak, M. M. *et al.* Quantification and restoration of the pre-drift extension across the NE Atlantic conjugate margins during the mid-Permian-early Cenozoic multi-rifting phases. *Tectonics*, e2022TC007386 (2023).

9 Gaina, C., Gernigon, L. & Ball, P. Palaeocene–Recent plate boundaries in the NE Atlantic and the formation of the Jan Mayen microcontinent. *Journal of the Geological Society* **166**, 601-616 (2009).

10 Torsvik, T. H. *et al.* Continental crust beneath southeast Iceland. *Proc Natl Acad Sci U S A* **112**, E1818-1827, doi:10.1073/pnas.1423099112 (2015).

11 Steinberger, B., Bredow, E., Lebedev, S., Schaeffer, A. & Torsvik, T. H. Widespread volcanism in the Greenland–North Atlantic region explained by the Iceland plume. *Nature Geoscience* **12**, 61-68, doi:10.1038/s41561-018-0251-0 (2018).

12 Lebedev, S., Schaeffer, A. J., Fullea, J. & Pease, V. Seismic tomography of the Arctic region: inferences for the thermal structure and evolution of the lithosphere. *Geological Society, London, Special Publications* **460**, 419-440 (2018).

13 Mordret, A. Uncovering the Iceland Hot Spot Track Beneath Greenland. *Journal of Geophysical Research: Solid Earth* **123**, 4922-4941, doi:10.1029/2017jb015104 (2018).

14 Toyokuni, G., Matsuno, T. & Zhao, D. P-Wave Tomography Beneath Greenland and Surrounding Regions: 2. Lower Mantle. *Journal of Geophysical Research: Solid Earth* **125**, doi:10.1029/2020jb019839 (2020).

15 Foulger, G. R. *et al.* The Iceland microcontinent and a continental Greenland-Iceland-Faroe ridge. *Earth-Science Reviews* **206**, 102926 (2020).

16 Gernigon, L. *et al.* A moderate melting model for the Vøring margin (Norway) based on structural observations and a thermo-kinematical modelling: Implication for the meaning of the lower crustal bodies. *Tectonophysics* **412**, 255-278 (2006).

17 Abdelmalak, M. M. *et al.* TheT-Reflection and the Deep Crustal Structure of the Vøring Margin, Offshore mid-Norway. *Tectonics* **36**, 2497-2523, doi:10.1002/2017tc004617 (2017).

18 Richardson, K., Smallwood, J., White, R., Snyder, D. & Maguire, P. Crustal structure beneath the Faroe Islands and the Faroe–Iceland ridge. *Tectonophysics* **300**, 159-180 (1998).

19 Holbrook, W. S. *et al.* Mantle thermal structure and active upwelling during continental breakup in the North Atlantic. *Earth and Planetary Science Letters* **190**, 251-266 (2001).

20 Förste, C. *et al.* EIGEN-6C4-The latest combined global gravity field model including GOCE data up to degree and order 1949 of GFZ Potsdam and GRGS Toulouse. *EGUGA*, 3707 (2014).

21 Ince, E. S. *et al.* ICGEM–15 years of successful collection and distribution of global gravitational models, associated services, and future plans. *Earth System Science Data* **11**, 647-674 (2019).

22 Amante, C. & Eakins, B. W. ETOPO1 1 ARC-MINUTE GLOBAL RELIEF MODEL: PROCEDURES, DATA SOURCES AND ANALYSIS. *NOAA Technical Memorandum NESDIS NGDC-24* (2009).

23 Kumar, A., Cacace, M., Scheck-Wenderoth, M., Götze, H. J. & Kaus, B. J. P. Present-Day Upper-Mantle Architecture of the Alps: Insights From Data-Driven Dynamic Modeling. *Geophysical Research Letters* **49**, doi:10.1029/2022gl099476 (2022).

24 Fichtner, A. *et al.* The Collaborative Seismic Earth Model: Generation 1. *Geophys Res Lett* **45**, 4007-4016, doi:10.1029/2018GL077338 (2018).

25 Gaina, C., Nasuti, A., Kimbell, G. S. & Blischke, A. Break-up and seafloor spreading domains in the NE Atlantic. *Geological Society, London, Special Publications* **447**, 393-417 (2017).

26 Lawver, L. A. & Müller, R. D. Iceland hotspot track. *Geology* **22**, 311-314 (1994).

27 Meza-Cala, J. C., Tsikalas, F., Faleide, J. I. & Abdelmalak, M. M. New insights into the late Mesozoic-Cenozoic tectono-stratigraphic evolution of the northern Lofoten-Vesterålen margin, offshore Norway. *Marine and Petroleum Geology* **134**, 105370 (2021).

28 Kumar, A. *et al.* LitMod2D_2. 0: An improved integrated geophysical-petrological modeling tool for the physical interpretation of upper mantle anomalies. *Geochemistry, Geophysics, Geosystems* **21**, e2019GC008777 (2020).

29 Rickers, F., Fichtner, A. & Trampert, J. The Iceland–Jan Mayen plume system and its impact on mantle dynamics in the North Atlantic region: Evidence from full-waveform inversion. *Earth and Planetary Science Letters* **367**, 39-51, doi:10.1016/j.epsl.2013.02.022 (2013).

30 Wolfe, C. J., VanDecar, J. C. & Solomon, S. C. Seismic structure of the Iceland mantle plume. *Nature* **385**, 245-247 (1997).

31 Barnett-Moore, N., Hassan, R., Flament, N. & Müller, D. The deep Earth origin of the Iceland plume and its effects on regional surface uplift and subsidence. *Solid Earth* **8**, 235-254, doi:10.5194/se-8-235-2017 (2017).

32 Tsikalas, F., Faleide, J. I., Eldholm, O. & Blaich, O. A. The NE Atlantic conjugate margins. *Regional geology and tectonics: Phanerozoic passive margins, cratonic basins and global tectonic maps* **1**, 140-201 (2012).

33 Brekke, H. The tectonic evolution of the Norwegian Sea continental margin, with emphasis on the Voring and More basins. *Special Publication-Geological Society of London* **167**, 327-378 (2000).

34 Van Wijk, J. & Cloetingh, S. Basin migration caused by slow lithospheric extension. *Earth and Planetary Science Letters* **198**, 275-288 (2002).

35 Skogseid, J. *et al.* NE Atlantic continental rifting and volcanic margin formation. *Geological Society, London, Special Publications* **167**, 295-326 (2000).

36 Dam, G., Larsen, M. & Sønderholm, M. Sedimentary response to mantle plumes: Implications from Paleocene onshore successions, West and East Greenland. *Geology* **26**, 207-210 (1998).

37 Planke, S., Rasmussen, T., Rey, S. S. & Myklebust, R. in *Geological Society, London, Petroleum Geology Conference series.* 833-844 (Geological Society of London).

38 White, R. S. Rift–plume interaction in the North Atlantic. *Philosophical Transactions of the Royal Society of London. Series A: Mathematical, Physical and Engineering Sciences* **355**, 319-339 (1997).

39 Jones, S. M., White, N., Clarke, B. J., Rowley, E. & Gallagher, K. Present and past influence of the Iceland Plume on sedimentation. *Geological Society, London, Special Publications* **196**, 13-25 (2002).

40 Bohnhoff, M. & Makris, J. Crustal structure of the southeastern Iceland-Faeroe Ridge (IFR) from wide aperture seismic data. *Journal of Geodynamics* **37**, 233-252, doi:10.1016/j.jog.2004.02.004 (2004).
41 Yuan, X., Korenaga, J., Holbrook, W. S. & Kelemen, P. B. Crustal Structure of the Greenland-Iceland Ridge from Joint Refraction and Reflection Seismic Tomography. *Journal of Geophysical Research: Solid Earth* **125**, doi:10.1029/2020jb019847 (2020).
42 Pilidou, S., Priestley, K., Debayle, E. & Gudmundsson, Ó. Rayleigh wave tomography in the North Atlantic: high resolution images of the Iceland, Azores and Eifel mantle plumes. *Lithos* **79**, 453-474, doi:10.1016/j.lithos.2004.09.012 (2005).
43 Celli, N. L., Lebedev, S., Schaeffer, A. J. & Gaina, C. The tilted Iceland Plume and its effect on the North Atlantic evolution and magmatism. *Earth and Planetary Science Letters* **569**, doi:10.1016/j.epsl.2021.117048 (2021).
44 Koptev, A., Cloetingh, S., Burov, E., Francois, T. & Gerya, T. Long-distance impact of Iceland plume on Norway's rifted margin. *Sci Rep* **7**, 10408, doi:10.1038/s41598-017-07523-y (2017).
45 Tan, P., Sippel, J., Breivik, A. J., Meeßen, C. & Scheck-Wenderoth, M. Lithospheric Control on Asthenospheric Flow From the Iceland Plume: 3-D Density Modeling of the Jan Mayen-East Greenland Region, NE Atlantic. *Journal of Geophysical Research: Solid Earth* **123**, 9223-9248, doi:10.1029/2018jb015634 (2018).
46 Schaeffer, A. J. & Lebedev, S. Global shear speed structure of the upper mantle and transition zone. *Geophysical Journal International* **194**, 417-449, doi:10.1093/gji/ggt095 (2013).

Methods

Apart from integration of structural characteristics derived from seismic and seismological imaging of the crust and mantle, diverse data compilations and previously built structural models, we additionally constrained the density distribution by three-dimensional gravity modelling. Gravity modelling was applied by forward calculating the gravity response of a certain density configuration using IGMAS+[47,48] and complemented by inverting the residuals found between observed and calculated gravity (Fatiando a Terra[49,50]). Details concerning all the integrated data and the modelling methodology are given in the SI.

The major interfaces compiled from seismic data and previous models and compilations are the top to the crystalline crust, the top of the high-velocity/high-density bodies located in the surroundings of the COT (COT-LCBs) and the crust-mantle boundary (Moho) (Figs. 2 b, i and c, respectively), as well as, the topography, bathymetry and the base of the ice (Fig. 2a). The thickness of the sedimentary deposits (Fig. 2d) was compiled from different sources (main source GlobSed v3[51], replaced by local higher resolution information in some regions[5,7,52,53]) detailed in SI. The thickness of the COT-LCBs unit was obtained from the compilation of [17] who interpreted a large seismic database from different sources. The depth to the Moho was compiled from several deep seismic data sets, receiver function studies and previously published compilations and models[52-56] (see more details in SI). To differentiate oceanic and continental domains, the COB compiled by [17] was considered.

In a first step, the units derived from data compilation were integrated into an initial 3D model with 7 layers, from top to bottom: water, ice, uniform sediments, uniform continental crust, uniform oceanic crust, COT-LCBs and uniform mantle. The scattered data describing the top surface elevation of the units were interpolated to obtain regular grids with a horizontal element spacing of 10 km (Convergent Interpolation algorithm of Petrel, ©Schlumberger, 2011.1.2). Further differentiation of the model in terms of spatial variations in crustal and mantle densities relied on additional deep seismic data sets. These contained depth information for major interfaces and seismic velocities that could be converted to densities. Within an iterative workflow of forward and inverse gravity modelling, we closed the gaps between the deep seismic information for which the velocity-derived densities were kept fixed. Thus, we sequentially refined the model always comparing it with the observed free-air gravity disturbances (EIGEN-6C4 at 6 km depth; Fig. 1b; more details in SI) following a stepwise procedure:

(1) Shear wave velocities of a tomographic model (an update of the Collaborative Seismic Earth Model CSEM[24]) were converted to temperatures and densities, using the Gibbs free-energy minimization method[57,58] through the Python application of [23]. A detailed description of the tomographic model, conversion method and the parameters involved is presented as SI.

(2) To account for compaction-driven density increase with depth, the sedimentary unit was divided into a shallow and a deep part (as detailed in the SI). The shallow portion above 8 km depth (below sea level) is considered as still possessing a degree of porosity and

thus a lower average density. Below 8 km depth, sediments are considered sufficiently compacted to have a higher average density.

(3) In the oceanic domain, several seismic profiles of the Greenland-Iceland-Faroe Ridge (GIFR) area image a thicker than normal layer 3 that additionally coincides with a positive gravity residual. Therefore, preserving the constraints given by the seismic information, we modelled the geometry of a high-velocity/ high-density body (GIFR layer 3) by fitting the observed gravity.

(4) The remaining gravity residuals in continental areas were inverted for crustal density variations. Deep refraction velocities along existing seismic profiles indicate that the continental crystalline crust is composed of an upper felsic and a lower mafic unit. The respective P-wave velocities were converted to average densities of the respective crustal interval and the interface between the felsic and the mafic continental crust was determined by inversion of the gravity residuals using a modified version of the Harvester module[50] of Fatiando a Terra[49].

Methods references

47 Götze, H.-J. & Lahmeyer, B. Application of three-dimensional interactie modeling in gravity and magnetics. *Geophysics* **53**, 1096-1108 (1988).

48 Anikiev, D. *et al.* IGMAS+: Interactive Gravity and Magnetic Application System. *Potsdam: GFZ Data services.* https://doi.org/10.5880/GFZ.4.5.igmas.v.1.3. (2020).

49 Uieda, L., Oliveira Jr, V. C. & Barbosa, V. C. in *Proceedings of the 12th Python in Science Conference.* 96-103.

50 Meeßen, C. *The thermal and rheological state of the Northern Argentinian foreland basins*, Universität Potsdam, (2019).

51 Straume, E. O. *et al.* GlobSed: Updated Total Sediment Thickness in the World's Oceans. *Geochemistry, Geophysics, Geosystems* **20**, 1756-1772, doi:10.1029/2018gc008115 (2019).

52 Klitzke, P., Faleide, J. I., Scheck-Wenderoth, M. & Sippel, J. A lithosphere-scale structural model of the Barents Sea and Kara Sea region. *Solid Earth* **6**, 153-172, doi:10.5194/se-6-153-2015 (2015).

53 Granath, J., Whittaker, R. & Dinkelman, M. Long offset seismic reflection data and the crustal structure of the NE Greenland Margin. *AGU Fall Meeting Abstracts.* T43G-2467.

54 Funck, T. *et al.* Moho and basement depth in the NE Atlantic Ocean based on seismic refraction data and receiver functions. *Geological Society, London, Special Publications* **447**, 207-231, doi:10.1144/sp447.1 (2017).

55 Petrov, O. *et al.* Crustal structure and tectonic model of the Arctic region. *Earth-Science Reviews* **154**, 29-71, doi:10.1016/j.earscirev.2015.11.013 (2016).

56 Maystrenko, Y. P., Bayer, U. & Scheck-Wenderoth, M. Regional-scale structural role of Permian salt within the Central European Basin System. *Geological Society, London, Special Publications* **363**, 409-430, doi:10.1144/sp363.19 (2012).
57 Connolly, J. A. D. Computation of phase equilibria by linear programming: A tool for geodynamic modeling and its application to subduction zone decarbonation. *Earth and Planetary Science Letters* **236**, 524-541, doi:10.1016/j.epsl.2005.04.033 (2005).
58 Connolly, J. A. D. The geodynamic equation of state: What and how. *Geochemistry, Geophysics, Geosystems* **10**, doi:10.1029/2009gc002540 (2009).

Acknowledgements: MLGD was partially supported by grants from the ESM-project of the Helmholtz Impulse and Networking Funds. MMA was funded by the Norwegian Petroleum Directorate (NPD) and Research Centre for Arctic Petroleum Exploration (ARCEx). JIF received support from the University of Oslo during his sabbatical at GFZ Potsdam.

We thank Dr. Christian Meeßen for his technical support during the data integration and gravity modelling procedure.

The 3D gravity modelling was carried out using IGMAS+ and Fatiando a Terra. For the visualization of results and the creation of figures various software packages were used: Paraview, MATLAB® version R2022b, Python (Python Software Foundation), ArcGIS and GMT (Wessel & Smith, 1991).

Author contributions: All authors together developed the research idea and evaluated the results. MLGD built the structural model, performed the gravity calculations and wrote the first version of manuscript. MSW supervised the modelling procedure and provided her proficiency to the drafting the manuscript. JIF contributed the expertise on the available data, most of the input data compilations and the geological history. JB co-supervised the data integration and the gravity modelling. MMA contributed with new interpretations of several seismic profiles and other available data and composed some of the Figures. DA helped to handle the data and visualize the results, including the composition of some Figures. All authors contributed to the discussion and interpretation of the results, revised the manuscript and were partially responsible for obtaining the financial support to develop this research.

Competing interest declaration: The authors declare no competing interests.

Additional information: Supplementary Information is available for this paper. Correspondence and requests for materials should be addressed to MLGD (gomezdacal@fcaglp.unlp.edu.ar).

Data availability: The results of this publication will be made available through the GFZ Data Services repository. The repository will include the geometry and density distributions.

Extended data – Figures and tables

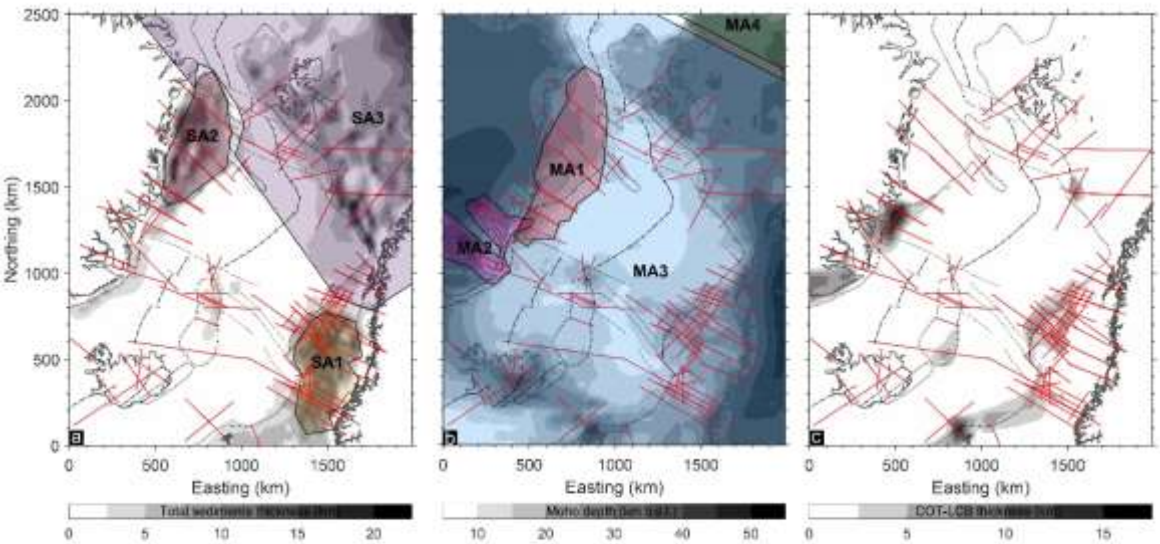

Extended data Figure 1. Data compilation for the initial model. a) Sedimentary thickness and the sources of information. The coloured areas limited by solid black lines are the regions with different data sources used to define the thickness of the sediments: SA1 area corresponds to [59], SA2 area to [53] and SA3 area to the model of [52]; b) Moho and the sources of information. Coloured areas limited by solid black lines indicate regions with different data sources used to define the Moho: MA1: [53]; MA2: [60]; MA3: NAGTec[54]; MA4: [52]. [55] and [56] are considered for the extended density model area only; c) High-velocity/high-density bodies in the surrounding of the COB (COT-LCBs). Red lines represent the location of seismic profiles utilized to define the respective surfaces.

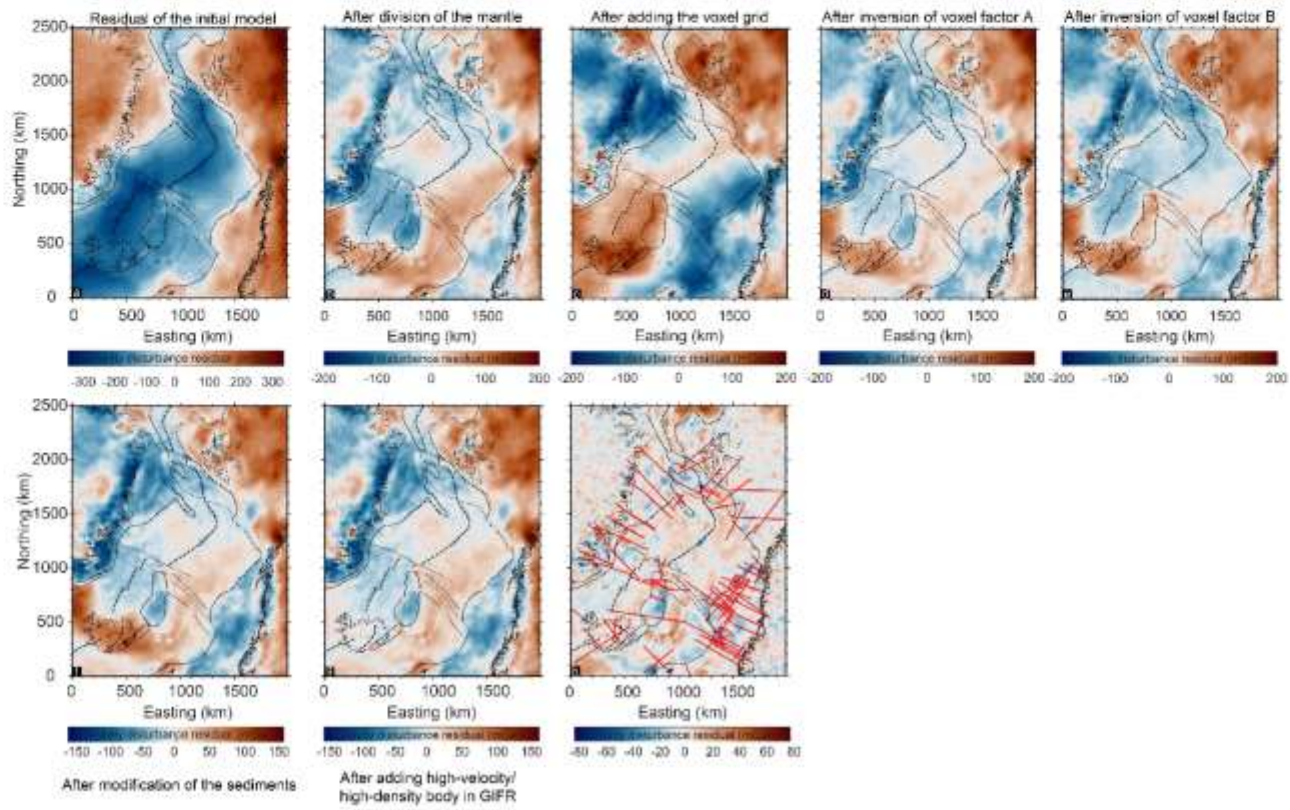

Extended data Figure 2. Residuals of the different modelling steps (See SI for details). a) Residuals of the initial model obtained by subtracting the gravity response of the initial 3D density model from the observed gravity field; b) Residuals after a division of the "Mantle" in two constant density domains (oceanic and continental mantle). c) Residuals after the incorporation of the voxel grid derived from the conversion from tomographic shear-wave velocities to densities. d) Residuals after the inversion of voxel factor "A" (using a two-domain-divided background density); e) Residuals after the inversion of voxel factor "B" (using a constant background density); f) Residuals after the refinement of the sedimentary layer; g) Residuals after the incorporation of the GIFR layer3 (Final forward modelling residuals); h) Residuals after inversion of the gravity residuals to split the crystalline crust in two layers: Final residuals of the model. Green lines are the locations of seismic profiles integrated as constraining information.

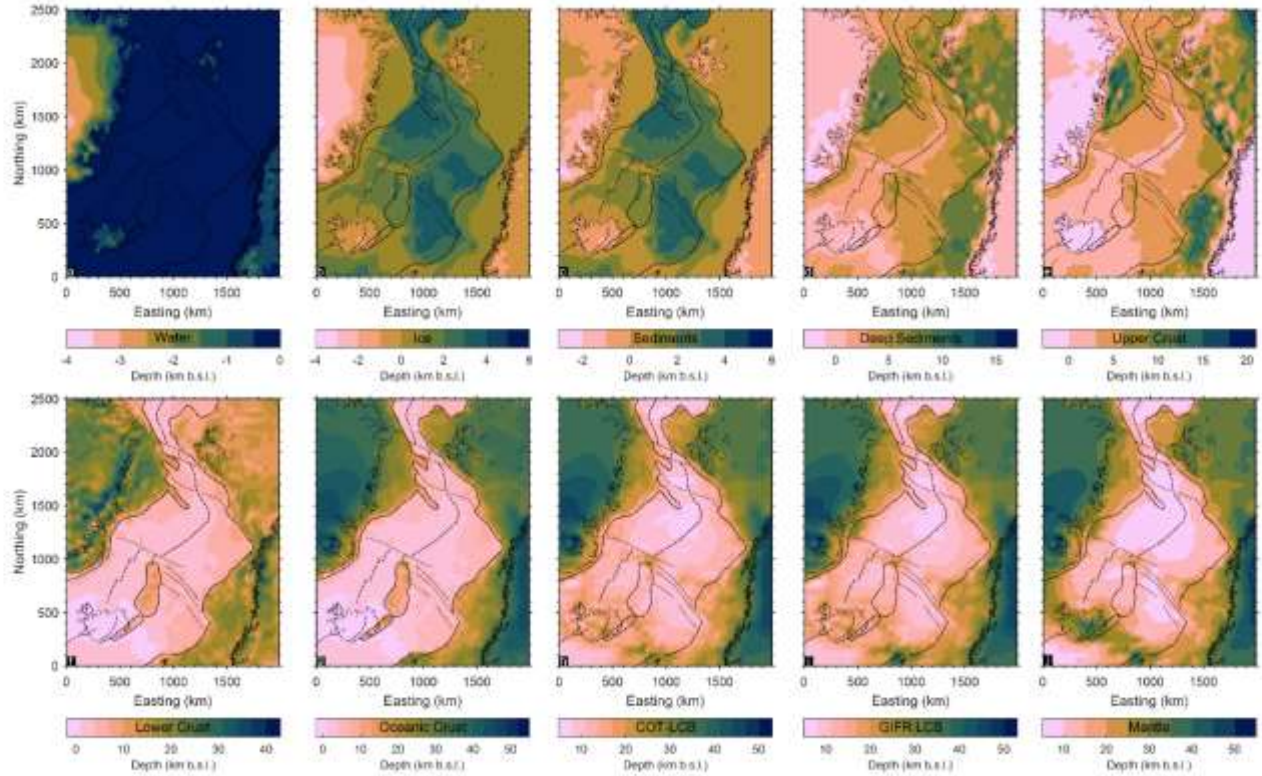

Extended data Figure 3. Structural interfaces (tops) of the units composing the final 3D structural model; a) upper surface of the model: top of the "Ice" sheets; b) top of the "Water"; c) top of the "Shallow sediments"; d) top of the "Deep sediments"; e) top of the "Upper crust": crystalline basement; f) top of the "Lower crust"; g) top of the "Oceanic crust"; h) top of the "COT-LCB"; i) top of the "GIFR layer3"; j) top of the "Mantle": Moho.

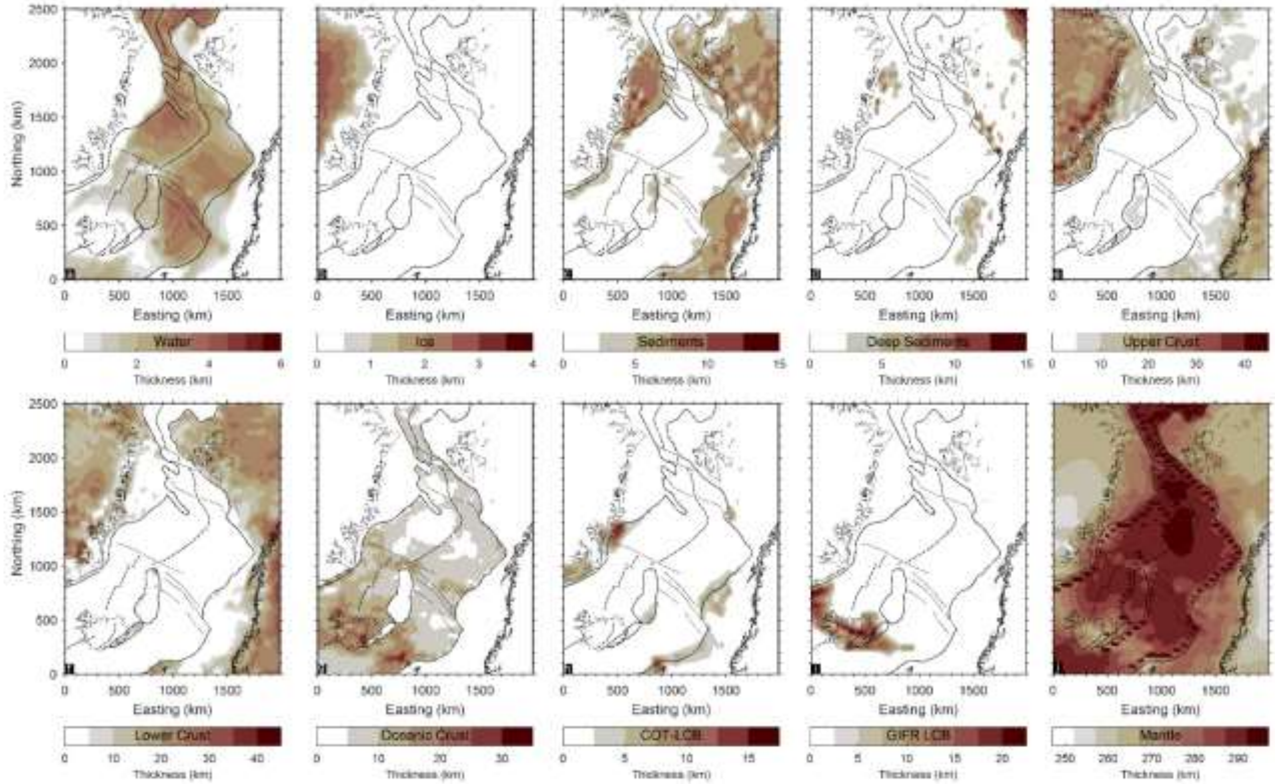

Extended data Figure 4. Thicknesses of the final model units. a) thickness of the “Ice”; b) thickness of the “Water”; c) thickness of the “Sediments”; d) thickness of the “Deep sediments”; e) thickness of the “Upper crust”; f) thickness of the “Lower crust”; g) thickness of the “Oceanic crust”; h) thickness of the “COT-LCB”; i) thickness of the “GIFR layer3”; j) thickness of the modelled “Mantle”: from Moho to 300 km depth.

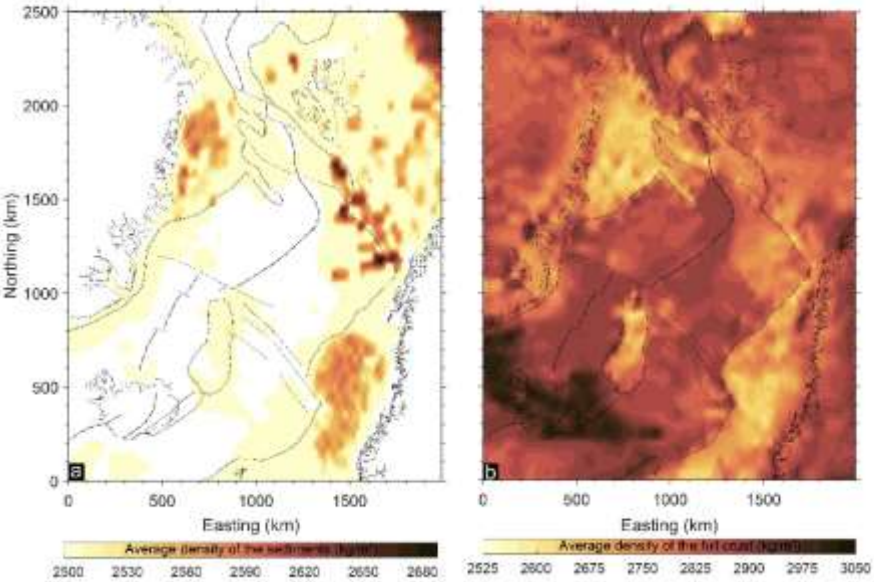

Extended data Figure 5. Complementary maps of crustal density distribution. a) Average density of the sediments: b) Average density of the full crust including both sedimentary units, upper and lower crust and high-velocity/high-density bodies.

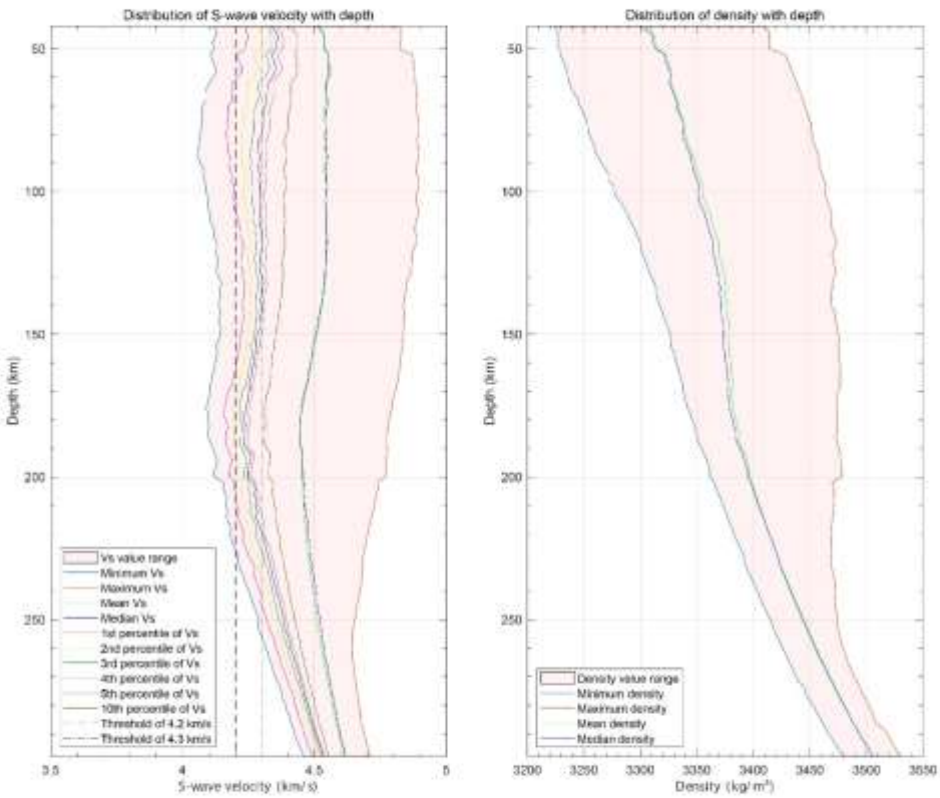

Extended data Figure 6. a) Distribution of the vs tomographic velocities and statistics for the model area; b) Converted densities that were included in the model, with respect to depth, and statistics.

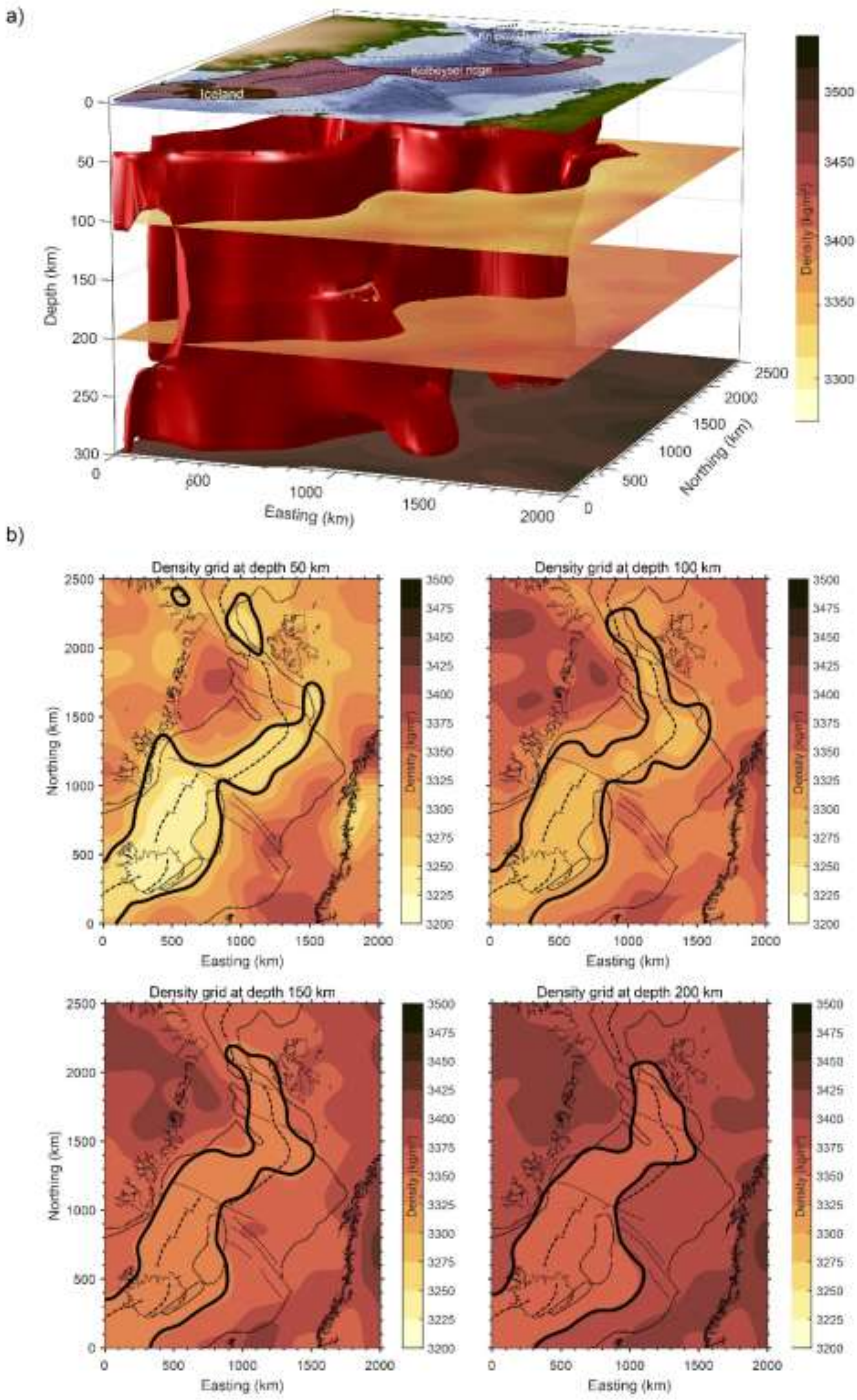

Extended data Figure 7. 10th percentile of lowest densities in the mantle as derived by converting S-wave velocities from the CSEM tomographic model (Generation 1[24]). a) 3D contouring and visualization with the topography/bathymetry of the region (ETOPO1[22]); b) 10th percentile contours on density slices at 50, 100, 150 and 200 km depth, respectively.

Surface/Layer	Sources	References
Topography + Top Ice + Sea Level	ETOPO 1	Amante and Eakins (2009)[22]
Ice thickness	ETOPO 1	Amante and Eakins (2009)[22]
Water thickness	ETOPO 1	Amante and Eakins (2009)[22]
Sediment thickness	GlobSed v3	Straume et al. (2019)[51]
	Klitzke et al. (2015)[52] model	Klitzke et al. (2015)[52]
	Interpreted seismic data in NE Greenland	Granath et al. (2011)[53]
	Thickness maps for Mid Norway	Zastrozhnov et al. (2020)[59]
	Seismic lines	Funck et al. (2017)[54]
Depth to Moho	NAGTec	Funck et al, (2017)[54]
	Klitzke et al. (2015)[52] model	Klitzke et al. (2015)[52]
	TeMar	Petrov et al. (2016)[55]
	Maystrenko et al., (2012)[56] model	Maystrenko et al. (2012)[56]
	Interpreted seismic data in NE Greenland	Granath et al. (2011)[53]
	Seismic profiles	Funck et al. (2017)[54]
	Receiver function central East Greenland	Kraft et al. (2019)[60]
Boundary between oceanic and continental crustal domains: COB	Compilation	Abdelmalak et al. (2017)[17]
Thickness of lower crustal bodies (LCBs) at the continent-ocean transition: "COT-LCB"	LCB thickness map	Abdelmalak et al. (2023)[8]

Extended data Table 1. Source information for the modelled geometries (surfaces and/or thicknesses) of the units of the initial 3D structural model.

Layer	Density (kg/m3)
Water	1030
Ice	920
Shallow sediments	2500
Deep sediments	2700
Upper continental crust	2700
Lower continental crust	3000
Oceanic crust	2900
COT-LCB	3000
GIFR layer 3	3100
Mantle	3D variable distribution

Extended data Table 2. Selected densities for the different units of the final model.

References Extended data

59 Zastrozhnov, D. et al. Regional structure and polyphased Cretaceous-Paleocene rift and basin development of the mid-Norwegian volcanic passive margin. *Marine and Petroleum Geology* **115**, 104269 (2020).Connolly

60 Kraft, H. A., Thybo, H., Vinnik, L. P. & Oreshin, S. Crustal structure in central-eastern Greenland from receiver functions. *Journal of Geophysical Research: Solid Earth* **124**, 1653-1670 (2019).

Supplementary Files

This is a list of supplementary files associated with this preprint. Click to download.

- SupplementaryInformationGomezDacal.docx